PCCP

Accepted Manuscript

ROYAL SOCIETY OF CHEMISTRY

www.rsc.org/pccp

Journal Name

RSCPublishing

ARTICLE

Experimental determination of electrostatic properties of Na-X zeolite from High Resolution X-Ray diffraction

Cite this: DOI: 10.1039/xoxxoooooox

Received ooth January 2012,
Accepted ooth January 2012

DOI: 10.1039/xoxxoooooox

www.rsc.org/

F. F. Porcher,[a,b] M. Souhassou[a] and C. E. P. Lecomte[a] ,

High-resolution single crystal X-ray diffraction is used for the first time to obtain the charge density distribution in dehydrated Na-X zeolite. The electron density is extracted according to Hansen & Coppens multipolar-model, from which P_{val}-κ-type atomic charges are derived. In order to compare the experimental electron density with theoretical calculations on zeolites and other minerals, a topological analysis is performed to derive AIM charges and electron density properties at bond critical points. The results are compared with that described in the literature. Finally, the electrostatic potential is evaluated in a periodic, mean field approach (disordered cation distribution in $Fd\bar{3}$ spacegroup) and for a given distribution of the cations (spacegroup P1). The electrostatic energy is, then, derived in the neighbourhood of cation sites where the molecules are usually physisorbed.

A Introduction

Faujasite (FAU) type zeolites are large pores zeolites widely used for gas separation, water softening, or catalysis. The unique properties of these zeolites are conditioned by their widely open topology (channel aperture ~7.4 Å) which allows easy diffusion of rather large guest molecules, and by the presence in their cavities of numerous, delocalized cations M^{q+} compensating the global charge defect due to the Si^{4+} ➔Al^{3+} substitution in the $(Si_xAl_{1-x})O_2$ framework. In peculiar, the sorption/exchange characteristics are more directly related to the localization of cations M^{q+}, while the catalytic properties are sensitive to the framework acidity and the Si/Al ratio. The different denominations of FAU zeolites (M-X for Si/Al < 1.5 and M-Y for Si/Al > 1.5) summarize efficiently these characteristics. Because of their very open structure, the FAU-type framework is prone to strong distortion upon cation exchange or sorption of guest molecules, which affects in turn the charge distribution. In addition, defects or framework substitution/acid sites are used for tuning the catalytic properties.

Because of their industrial impact, a large effort is devoted to the comprehensive modelling the physisorption properties of FAU zeolites at the atomic-scale. The size of the system (~700 atoms per unit cell for the zeolite itself) precludes accurate *ab initio* calculations, and sorption and self-diffusion are modelled by molecular dynamics or Monte-Carlo simulations, assuming e.g. a rigid $AlO_2SiO_2^{q-}$ framework [Ramanan *et al.,* 2004], [Wander *et al*., 2006]. Depending on the problem addressed (cation exchange, sorption of neutral polar or apolar molecules) a large variety of force-fields was developed, tuned to reproduce macroscopic properties (exchange enthalpy, adsorption isotherms,…). For example, in the case of highly polar zeolites M-X or M-A with topology FAU and LTA respectively, the Coulombian and polarization terms override the dispersion and repulsion ones, hence the importance of a thorough estimation of partial charges. In the present study, we show how high resolution X-ray diffraction can be used to model the electron density in Na-X, which is the pristine form of X-type zeolites and one of the more widely used sorbent. After a brief description of the sample and experimental setting, we will present the specific difficulties in deriving the experimental electron density on zeolites, where the relative ratio between core and valence electrons, $\rho_{core}(r)/\rho_{val}(r)$, is less favourable than in mostly studied organic molecules, and where large atomic displacement parameters complicate the deconvolution of thermal parameters (ADPs). A thorough data analysis, together with specific constrains in the multipolar parameters, are needed in such systems before atomic charges and electrostatic potential are calculated. Finally, the calculated electrostatic energy of water molecules sorbed at different cation sites will be compared with the extensive literature available for Na-X.

B Experimental Details

A Sample preparation and characterization.

Charge density determination can only be performed on samples of good crystalline quality and when an accurate

structural model is available, with limited disorder or thermal motion. In the case of basic X-type zeolites, the numerous monovalent charge-compensating cations are largely disordered in the cavities but as long as Si/Al ~1, the Si-Al substitution on tetrahedral sites is limited. In this case, SiO_4 and AlO_4^- tetrahedra alternate regularly in the structure in agreement with Löwenstein [Löwenstein, 1954] rule and the crystallographic space group is $Fd\bar{3}$, while for Si/Al > 1.2 disorder on Si/Al sites induces the more symmetrical $Fd\bar{3}m$ space group.

From the synthesis point of view, two protocols may be used to grow sample with Si/Al ~1 : Kühl's method using a mixture of Na^+/K^+ cations, providing only powder [Kühl, 1987], or Charnell's method using only Na^+ as charge compensating cation and providing small single crystals [Charnell, 1971]. This latter method was modified [Porcher, 1998] in order to produce large (~100µm) single crystals with an Si/Al ratio estimated to 1.06 from ^{29}Si and ^{27}Al nuclear magnetic resonance (NMR) and microprobe analyses. The chemical formula, $Na_{93}Al_{93}Si_{99}O_{384}$, assumes a formal Na/Al value of unity as the migration of cations under the electron beam precludes estimation of Na^+ content by microprobe.

For the experiment, selected colourless and transparent single crystals were dehydrated for 6 days under secondary vacuum and heating according to the protocol described in [Porcher, 1998]. ^1H NMR analysis confirmed the dehydration (less than 0.03 wt% H_2O) while the framework's preservation during dehydration was checked by ^{27}Al NMR which spectrum did not exhibit any characteristic signal of octahedral-coordinated aluminium atom (Suppl. Fig. 1a).

The local Si/Al ordering on tetrahedral sites was confirmed by ^{29}Si NMR spectrum which only showed the Q4(4Al) peak (Suppl. Fig. 1b). $Fd\bar{3}$ crystal symmetry was assessed by the higher internal agreement in $Fd\bar{3}m$ space-group compared to $Fd\bar{3}$, and by the difference between the Si-O and Al-O bond lengths as shown in Table 3.

B Data collection and reduction.

Charge density studies are particularly difficult to realize on FAU-type zeolites because of their weak diffracting power (density d~ 1.5, to be compared with d~2-3 for usual silicates) which often preclude accurate high resolution data collection ($\sin\theta/\lambda>0.8 Å^{-1}$). The estimation of precise standard deviations on weak I(hkl) Bragg intensities is of first importance, since these reflections are the most abundant in the high resolution shells used for the deconvolution of structural/deformation atomic parameters (see section D).

In this goal, a first dataset was collected on a Na-X single crystal on beamline ID11 at the ESRF synchrotron using a first generation of CCD detector (Bruker SMART). The measurement was overall satisfying, but suffered of the fluctuation of the synchrotron beam, and of unreliable estimation of standard uncertainty because of the limited redundancy (r=6.3) of the dataset. Progress in instrumentation made possible, few years after, to collect a good quality dataset on a conventional source (Oxford Xcalibur CCD diffractometer at CRM^2, Nancy, France). Forty-eight symmetry equivalent reflections were measured, up to $\sin\theta/\lambda$~1.06Å^{-1}. However, 4 unique low order reflections (1 1 1, 2 2 0, 2 2 2 and 3 1 1) important for the modelling of the charge density were shaded by the beam stop and missing, reducing the completeness to 92.7% for $0<\sin\theta/\lambda<1.06$ Å^{-1}. The measurement was performed at 100K in order to reduce atomic displacement parameters (ADPs). An empirical absorption correction was applied using SORTAV program [Blessing, 1995] before data reduction and estimation of standard uncertainty of unique reflections assuming a Poissonian distribution of their equivalents [Petricek *et al.* 2006,].

Subsequent analysis of the intensities on both datasets (see section D) revealed that the weakest reflections were systematically overestimated and had to be discarded from the least-square refinements. Diffraction details for these experiments are summarized in Table 1. Hereafter, the refinement procedure will be discussed solely for the CRM^2 data, which appeared to be of better quality due to its redundancy, but a similar strategy was adopted for the ESRF data.

C X-ray crystallography and modelling of electron density.

X-rays interact predominantly with the electrons of the matter, and the structure factors ($F(\vec{H})$ are the Fourier components of the electron density (ED). For conventional structure determination by XRD, a limited sampling of the reciprocal space at medium resolution is performed, as the atomic positions $\vec{r}$ can be estimated from the maxima of the smeared, reconstructed electron density.

Table 1 Data collection details

XRD dataset	ID11 (ESRF)	CRM^2 (Nancy)
Temperature	293K	100K
X-Ray source	Synchrotron	Mo(Kα) tube
Wavelength	0.248Å	0.709Å
Diffractometer	Bruker SMART	Oxford XCalibur
(software)	CCD (SAINT)	CCD (Crysalys)
Max. Resolution $\sin\theta/\lambda$	1.37Å^{-1}	1.06Å^{-1}
Reflections measured	73685	306049
Completeness ($\sin_{q/I\|max}$)	82.7%	92.7%
$\sin\theta/\lambda$ (99.9% compl.)	1.15Å^{-1}	1.02Å^{-1}
R_{int} / $R_{w,int}$	0.073 / 0.050	0.135 / 0.073
Redundancy	6.3	48.0
Unique ref. before rejection	11693	6437
Ref. for Refinement / R_{free}	10070 / 508	1871 / 105

[a] $R_{int} = \sqrt{\frac{N}{N-1}} \sum_{\vec{H}} \sum_{\vec{H}'} \left| \frac{I(\vec{H}') - \langle I(\vec{H}) \rangle}{I(\vec{H}')} \right|$ $\quad Rw_{int} = \sqrt{\frac{N}{N-1} \sum_{\vec{H}} \sum_{\vec{H}'} \frac{\left(\frac{I(\vec{H}') - \langle I(\vec{H}) \rangle}{\sigma(I(\vec{H}'))} \right)^2}{\left(\frac{I(\vec{H}')}{\sigma(I(\vec{H}'))} \right)^2}}$

where $\vec{H}$ runs over all independent reflections and $\vec{H}$' over the N reflections equivalent by symmetry to $\vec{H}$.

In order to access to information on charge transfer and covalent bonding, higher resolution structure factors are needed, for a proper deconvolution from structural features [Coppens, 1997]. The classical decomposition of ED over unperturbed pseudoatomic densities is no longer pertinent and

more complex models (continuous density via Maximum Entropy Method [Sakata & Sato, 1990] [De Vries *et al*., 1996], multipolar decompositions [Stewart, 1969], multicentered density) are needed. For example, the Hansen–Coppens model [Hansen, 1978] used is this study expresses each pseudoatom density as:

$$\rho_{at}(r) = \rho_{core}(r) + \rho_{val}(r) \quad (1)$$

with

$$\rho_{val}(r) = P_{val}\,\kappa^3\,\rho_{val}(\kappa r) + \Sigma_l \Sigma_m\,\kappa'^3\,R_{nl}(\kappa' r)\,P_{lm}\,Y_{lmp}(\theta,\phi) \quad (2)$$

where ρ_{core} and ρ_{val} are, respectively, Hartree-Fock spherical core and valence density (ρ_{val} being normalized to one electron). In this expression, Y_{lmp} are the spherical harmonic angular functions of order l in real form and $R_{nl}(r)$

$$R_{nl}(r) = N_{nl}\,r^n\,e^{-\zeta r}$$

are Slater type radial functions normalized with N_{nl}.

The parameter refined against XRD data are

- the valence population parameter P_{val} , which gives the atomic charge and the iconicity of the atoms.
  The "P_{val}-κ" net charge is $q = N_{val} - P_{val}$
  where N_{val} is the nominal valence.
- the P_{lm} multipolar population parameters, that describe the asphericity of the electron density (accumulation of electrons in covalent bonds, lone pairs)
- the κ and κ' contraction/expansion coefficients for respectively spherical and multipolar valence densities.

Multipolar modelling of atomic densities is extended up to order 4 (hexadecapoles) for Si, Al and to order 3 (octopoles) for oxygen atoms. Conventional values were chosen for n and ζ parameters of the radial function (Suppl. Table 1).

D Multipolar refinement of electron density in Na-X.

As FAU-type zeolites have peculiar difficulties (as described in the Introduction), the following refinement strategy was followed.

For the Na atom, the valence scattering factor $f_{val}(\sin\theta/\lambda)$ falls to zero at $\sin\theta/\lambda \sim 0.15$ Å^{-1} (Fig. 1), which precludes any charge density refinement because of the too low number of contributing Bragg reflections.

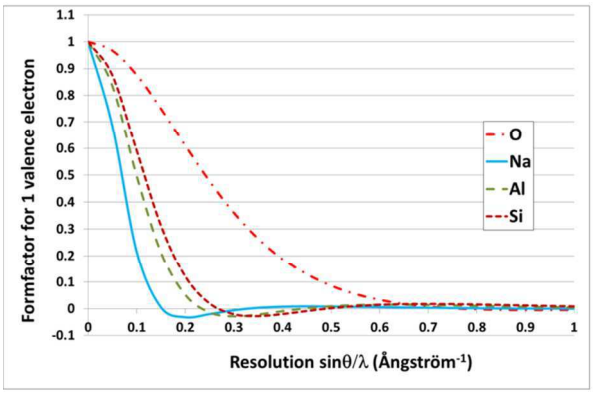

Fig. 1 Valence formfactor of Si, Al, Na, O atoms

A +1 charge was assumed, then, which is compensated by an –1 charge distribution over the framework atoms. For Al, and to a lesser extent for Si, the valence information is concentrated in the 0 - 0.3Å^{-1} reciprocal shell and extraction of multipolar parameter remains tedious. As a contrary, refinement of multipolar parameters for oxygen atoms is easier since these latter have significant $f_{val}(\sin\theta/\lambda)/f_{core}(\sin\theta/\lambda)$ ratio up to $\sin\theta/\lambda$ =0.9A^{-1}, and therefore stabilize the multipolar refinement.

For this study, geometrical constraints were imposed on multipolar P_{lm} parameters along the refinement, assuming ideal tetrahedral -43*m* symmetry for Si and Al atoms, and *mm*2 symmetry for bridging oxygen atoms, notwithstanding their slightly asymmetric coordination with Si in one side and Al the other one. In this goal, convenient local cartesian axes were chosen for the definition of spherical harmonic (Suppl. Fig. 2) in order to impose an additional constraint with identical P_{lm} parameters for all four oxygen atoms. These constraints are implemented in the refinement software JANA [Petricek *et al*., 2006]

According to these specific difficulties, the following refinement strategy was adopted:

Step 0) Test IAM refinement using observed reflections with (I(hkl) > 1σ(I(hkl)) in order to check the consistence of the observed I_{obs} and calculated I_{calc} intensities. This step clearly reveals an anomaly in the estimation of weak structure factors (Fig. 2) that were systematically overestimated during the integration of the diffraction images, as were those from the ESRF experiment. These latter (I_{obs} < 70) were then discarded from the following refinements. The remaining data were split in two sets, with 95% of the reflections used for the refinement and 5% reserved for the calculation of a control R_{free} factor ([Brünger, 1992] [Zarychta *et al*., 2011]).

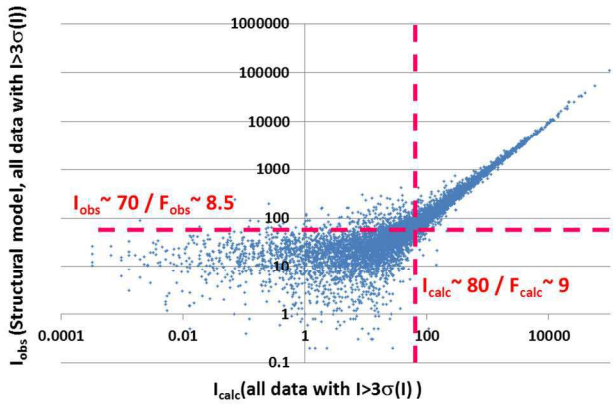

Fig. 2 Observed (I_{obs}) and Calculated (I_{calc}) Bragg intensities at the end of the test refinement (Step 0), CRM^2 dataset). The rejection limit (I_{calc}(hkl) <80) is plotted in red.

Step 1) Conventional structure refinement using the reflections selected at Step 0).
Displacement parameters are neatly higher (U_{iso}~0.033Å^2 for O atoms) than those refined for natural zeolites (U_{iso}~0.012 Å^2 for O atoms in Natrolite ([Ghermani *et al.*, .1996], [Kutzinger *et al.*, 1998]).

Step 2) Constrained "P_{val}-κ" refinement assuming the same expansion-contraction coefficient κ for all oxygen atoms and electroneutrality in the cell and fixed (Step 2a) or refined (Step 2b) structural parameters. Because of the shape of Al valence scattering factor (Fig. 1), the κ(Al) parameter was not refined. Varying its value in the 0.85-1.15 range drives the P_{val} parameter from 2.3 to 1.5 without changing the significantly P_{val} values of Si and O atoms by more than 0.15 nor the refinement statistics. Such a problem has already been discussed by Pérès *et al*. [Pérès *et al.*, 1999].
Therefore the κ-value was set to 1 and the electroneutrality constraint leads to a better estimation of P_{val}(Al) ~1.86(0.16) and a lower value of the dispersion on the four oxygen atoms $<P_{val}(O)>$ = 0.8±0.1. All P_{val}-κ parameters and atomics charges are given in Table 4.
As refining atomic positions and Debye–Waller parameters without multipolar parameters led to better reasonable P_{val} and κ values, Step 2b was discarded.

Step 3) Multipolar refinement assuming identical deformation parameters for all O atoms and local symmetry constraints for Si, Al and O atoms. In Step 3a, atomic coordinates and displacement parameters are frozen, then are released in Step 3b. Any attempt to unconstrain multipolar parameters of the four oxygen atoms (Step 3c, Suppl. Fig 3) or relax local symmetry constraints was unsuccessful and produced meaningless densities.

The evolution of the agreement factors along the various refinement steps is summarized in Table 2. The improvement of the R_{free} parameter confirms the quality of the multipolar refinement [Zarychta *et al.*, 2011].

Table 2 Agreement factors at various refinement steps for CRM^2 dataset (see Text for details). The main dataset comprises 1871 reflections (95%) while 105 reflections (5%) are reserved for R_{free} calculation.

Step	R	R_w	Gof	R_{free}	$R_{w,Free}$
1	5.34	6.40	1.16	5.72	6.38
2a	5.20	6.18	1.10	5.73	6.37
2b	5.19	6.13	1.12	5.79	6.45
3a	5.20	6.06	1.08	5.61	5.85
3b	5.14	6.00	1.09	5.51	5.59

[a] Agreement factors are defined as :

$$R = \frac{\Sigma|F_{obs}|-|F_{calc}|}{\Sigma|F_{obs}|} \quad \text{and} \quad R_w = \sqrt{\frac{\Sigma w(|F_{obs}|-|F_{calc}|)^2}{\Sigma|F_{obs}|^2}}$$

$$Gof = \sqrt{\frac{w(F_{obs}-F_{calc})^2}{m-n}} \quad \text{with} \quad w = \frac{1}{\sigma^2(F_{obs})}$$

and m, n number of reflections and n parameters refined

F_{calc}, F_{obs}: Calculated and rescaled measured structure factors.

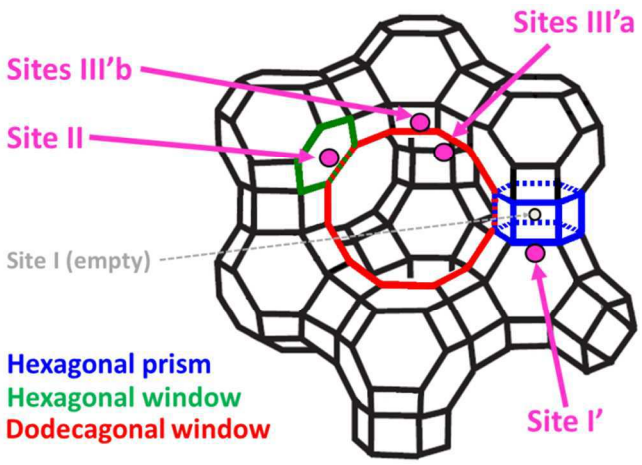

Fig. 3 Cation sites in FAU zeolite

C Results and discussion: Electrostatic properties of Na-X zeolite

A Crystal structure and cation distribution.

The cation distribution is similar with that found previously in the room temperature single crystal XRD study [Porcher, 1999 and references therein]. Na^+ cations sit on four different sites (Fig. 3) called sites I', II, III'a and III'b, with refined occupancies of 17.1(3)% (site III'a) and 16.2(3)% (site III'b) as compared to 16(1) and 18(2) for the RT study.

- Cations Na1 in sites I' lie inside the sodalite cage and are inaccessible to sorbed molecules. Each Na1 is coordinated to three O3 oxygen atoms of a hexagonal prism with Na1-O3=2.233(4) Å.
- Cations Na2 in sites II are inside the supercage, close to hexagonal window. These are bound in the same fashion as Na1 to three O2 oxygen atoms of a six-membered ring (Na2-O2=2.315(4) Å).

Cations Na3 and Na4 occupy statistically sites III'a and III'b and they are disordered about the dodecagonal window in the supercage and are highly accessible to guest molecules. Their coordination is relatively loose. Na3 is only coordinated to one O4 oxygen (Na3-O4=2.10(1) Å), and is at 2.74(1) and 2.78(1) Å of two O1 atoms. Na4 interacts only with two O4 and one O3 oxygen atom at 2.72(9), 2.74(9) and 2.95(9) Å. These weak interactions explain their lability when guest molecules are adsorbed. The abnormally large thermal displacement parameter of Na3 suggests an additional disorder along O1…O1 axis.

B Electron density distribution.

Multipolar modelling provides Δρ static deformation density maps that illustrate the deformation of valence cloud induced by chemical bonding:

$$\Delta\rho_{stat}(\vec{r}) = \kappa'^{3} P_{val}.\rho_{val}(\kappa.r) - N\rho_{val}(r) + \sum_{l}\sum_{m} \kappa'^{3} R_{nl}(\kappa'.r).P_{lm}.Y_{lm\pm}(\theta,\phi) \quad (3)$$

Such maps are very sensitive to the quality of the least-squares refinement, and, in particular, to the correlation between positional and multipolar parameters. This problem was eliminated when the P_{lm} parameters of O3 atom are constrained to those of other oxygen atoms. Fig. 4 and Fig. 5 present the maps at the end of the refinement (Step 3b) for CRM^2 dataset around the bridging oxygen O2 and in the hexagonal window and hexagonal prism. Suppl. Fig. 4 show the same maps for the ESRF dataset; which are qualitatively similar. The static deformation density around O atoms exhibits most typical features observed in other minerals: accumulation of density in Si-O and Al-O bonds and a bulge at lone pair position on the external side of the Si–O–Al angle.

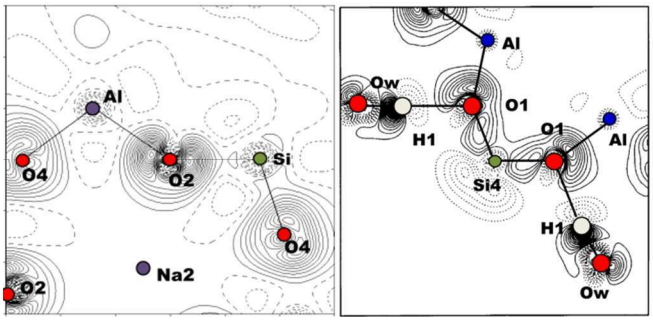

Fig. 4 Static deformation density maps calculated at the end of the refinement (Step 3b, CRM^2 dataset) in the Si-O2-Al plane of Na-X (a) and in the Si4-O1-Al plane of Natrolite (b) - contours 0.05e/Å^3.

The deformation density in the T-O bonds in Na-X (Fig 4a) is similar to that obtained in Natrolite (Fig 4b, [Ghermani *et al*., .1996] and other zeolites ([Kutzinger *et al*., 1998], [Kirfel & Gibbs, 2000]). The O2 lone pair is polarized toward the Na2 cation and stabilizes it. Similar features are observed for O3 and O4 that coordinate the other Na^+ cations. In all cases, the Na…O interaction is almost aligned with the bisector of the Si-O-Al angle, but slightly displaced toward Al, as expected since the Al-O distance is longer (1.72 Å) than Si-O (1.62 Å). This feature is clearly seen on the deformation maps in the zeolite hexagonal windows (Fig. 5).

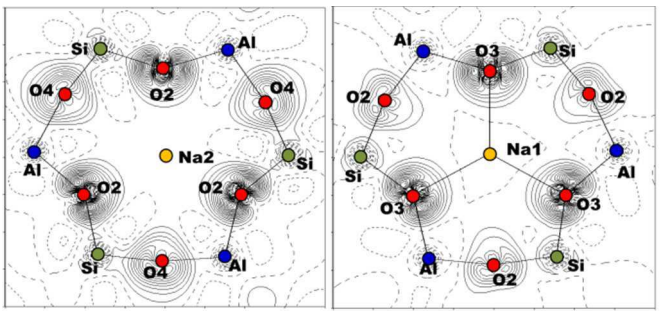

Fig. 5 Static deformation density maps calculated at the end of the refinement (Step 3b, CRM^2 dataset) in the O2-O2-O2 plane of the hexagonal window (a) and the O3-O3-O3 plane of the hexagonal prism (b). (contours 0.05e/Å^3).

C Topological analysis of electron density.

"Atoms In Molecules" (AIM) analysis [Bader, 1990] facilitates the quantitative analysis of electron density by focusing it on the "Critical Points" (CP) located at positions $\vec{r_c}$ where $\vec{\nabla}(\vec{r})$ vanishes. These CP are classified by the rank r and signature σ of the Hessian matrix of $\rho(\vec{r_c})$ and labelled (r, σ). The (3, -1) saddle-type critical points characterise the bonding interactions between atoms. AIM analysis provides also an unambiguous definition of atomic charges and moments, valuable whatever the origin (experimental or theoretical) of the ED [Souhassou & Blessing, 1999].

Table 3 lists the bond critical points between framework atoms in Na-X, compared to those in NAT-type zeolites. As expected, the critical points in Si-O and Al-O bonds sit on the T-O axes (d(O)+d(T)~d(T-O)), and are closer to the electropositive T-atoms. Electron density at critical point is higher in Si-O bonds (ρ(3,-1) ~0.9e/Å^3) than in Al-O ones (ρ(3,-1) ~0.6e/Å^3), in line with the more covalent character of Si-O bonds. The oxygen bounded radius, given by the distance between the critical point and O nuclear position, is equal to that measured in NAT-type zeolites (dO~0.93Å). The density at critical point (ρ(3,-1) ~0.93e/Å^3 in Na-X) is slightly weaker compared to ρ(3,-1) ~1.05e/Å^3 in NAT-type zeolites), despite similar or even shorter Si-O/Al-O bonds. It stays, however, well in the range of the value obtained in other aluminosilicates, from experimental or theoretical charge density modelling: ρ (3,-1) =0.90-1.05e/Å^3 for Si-O distances ranging between 1.64-1.60 Å [Gibbs *et al*., 2009]. This trend reflects the greater extension of oxygens atomic basins which protrude far inside the zeolite cavities, as far as to ~3.5 Å away of the nucleus. The laplacian values are in line with those obtained in other aluminosilicates ("closed-shell" interaction between Si-O and Al-O, with predominant ionic character).

Table 3 Topological properties at bond critical points in the framework of Na-X zeolite and in Natrolite, Scolecite and Masolite NAT-type zeolite [A. Kirfel, & G. Gibbs, 2000].

T-O	Si-O1	Si-O2	Si-O3	Si-O4	Al-O1	Al-O2	Al-O3	Al-O4
d(T-O)	1.608	1.631	1.632	1.620	1.699	1.729	1.734	1.708
d(T)	0.684	0.692	0.694	0.681	0.744	0.750	0.753	0.739
d(O)	0.923	0.941	0.942	0.935	0.966	0.977	0.983	0.971
ρ(3,-1)	0.91	0.87	0.85	0.96	0.61	0.59	0.56	0.65
Lap(ρ)	23.28	20.81	20.90	22.88	19.33	18.21	17.79	19.88

NAT-type zeolites

	Natrolite		Mesolite		Scolecite	
	Si-O	Al-O	Si-O	Al-O	Si-O	Al-O
d(T-O)	1.620	1.742	1.621	1.743	1.620	1.746
ρ(3,-1)	1.018	0.658	1.053	0.710	1.090	0.670
Lap(ρ)	14.12	14.81	10.48	10.76	12.69	12.31
d(O)	0.938	0.998	0.939	0.999	0.939	1.010

[a] For NAT-type zeolites, topological properties are the average of many Si-O and Al-O bonds.

The coordination of Na^+ cations by the framework oxygen atoms is assessed by the existence of (3, -1) critical points in the Na…O line: the strong interaction between Na1 and six oxygen atoms O3 of hexagonal prism gives rise to a rather high electron density at critical point (0.16 e-/Å^3), similar to that (0.13 e-/Å^3) found between Na2 and three O2. For disordered site III' cations with weak occupancy factor, a clear critical point is only evidenced in the short bond between Na3 and O4 (0.13 e-/Å^3). More disputable critical points with a density less than 0.07 e/Å^3 are found in the Na-O bonds longer than 2.5 Å.

D Atomic charges in NaX: a summary.

In order to allow comparison with theoretical ED calculations, topological charges were calculated by integration of $\rho(\vec{r})$ over their atomic basins Ω as defined by their zero flux surfaces:

$$\Omega(\rho(\vec{r})): \quad \vec{\nabla}(\vec{r}).\vec{n}(\vec{r}) = 0$$

The resulting AIM charges are given in Table 4 together with the κ-charges from P_{val}-κ refinement and that derived by the Electronegativity Equalization Method (EEM) [Mortier *et al*., 1986]. In this later method, charges are derived from the change of atomic electronegativities during bond formation and from geometrical effects assuming a Coulombic correction term.

The P_{val}-κ charges obtained at low temperature (CRM^2) or RT (ESRF dataset) are identical within the error bars. Clearly, these charges are close to that derived from EEM analysis [Uytterhoeven *et al*, 1992], [Di Lella *et al*., 2006]; within the experimental accuracy, the oxygen charges cannot be differentiated: q(O)=0.83e-. They are also similar to those obtained in Quartz by Guillot [Guillot 2002] but are less contrasted than those obtained in NAT-type zeolites. The difference on the charges comes from the different structure of Na-X zeolite (with FAU topology) and Natrolite and Scolecite (which share the same NAT topology), together with their Si/Al ratio. As explained by Ghermani *et al.* for the Natrolite, the charges of the oxygen atoms, which drive that on Si and Al atoms, are influenced by the presence of interacting Na^+ cations. In Natrolite, the strong charge of the O2 atom (-1.21) is explained by ionic bonds to two Na cations [Ghermani *et al*., 1999]. The charge of O3 and O4, which are linked to only one Na^+ cation is about -1.05(5). O1 and O5, which do not coordinate Na^+ cations, but only water molecules, bear -0.90(5) and -0.87(5) charges, respectively. The values of the charges found in Na-X are in this order of magnitude, accounting for the fact that the coordination of cations Na1 and Na2 is shared by 3 oxygens and that Na3 and Na4 are highly disordered and have a very partial occupancy factor of about 17%.

The structure of Natrolite $Na_2Al_2Si_3O_{10}.2H_2O$ is also more ionic than that of Na-X, with a greater Al/Si ratio, hence a greater Na^+/Si ratio, and, as could be expected, larger atomic charges on oxygen atoms. These charges influence softer Al and Si atoms which are more cationic in Natrolite than in Faujasite. Notwithstanding these structural differences, the global values remain comparable in both cases.

The AIM charges of O atoms (~1.6$^-$) are in line with those obtained by Gibbs *et al*. for α–SiO_2 [Gibbs *et al*., 1999] and, more generally, with that obtained in other aluminosilicates. The charges of the neighbouring Si, Al cations compensate them, according to their respective iconicity and to the geometry of the Si-O / Al-O bonds and Si-O-Al valence angles.

Table 4 Atomic charges in Na-X (this study), NAT-type zeolites [Ghermani *et al*., 1996], [Kutzinger *et al*., 1998] and Quartz [Guillot *et al*., 2002], [Gibbs *et al*., 1999].

Type	Si	Al	O1	O2	O3	O4	Na
P_{val}-κ (CRM^2)	+1.2(2)	+1.2(3)	-0.82(8)	-0.84(9)	-0.74(9)	-0.91(9)	+1
P_{val} -κ (ESRF)	+1.3(2)	+1.0(-)	-0.7(1)	-1.0(1)	-0.7(1)	-0.9(1)	+1
EEM	+1.3	+1.1	-0.83	-0.91	-0.90	-0.87	+1
AIM	+2.52	+2.26	-1.54	-1.62	-1.23	-1.60	0.19(6)
Natrolite	+1.9(1)	+1.5(1)	-0.90(5)	-1.21(5)	-1.03(5)	-1.07(5)	+1
P_{val} -κ	+1.6(1)		-0.87(5)				(Na)
Scolecite	+2.1(1)	+1.9(1)	-1.15(9)	-1.39(9)	-1.31(8)	-1.21(8)	+2
P_{val} -κ	+1.8(1)	+1.9(1)	-1.31(9)	-0.95(8)	-1.00(9)	-1.00(8)	(Ca)
	+1.7(1)		-0.89(7)	-1.24(8)			
Quartz P_{val} -κ	+1.2(1)		-0.6(1)				
Quartz AIM	+3.20		-1.60				

[a] Value of κ parameter for P_{val}-κ charges are :

Si : 1.06(4), Al : 1.00, O:0.954(7) (CRM^2 dataset)

For AIM charges in Na-X, the average value of q(Na) is given.

D Electrostatic Potential in Na-X.

Electrostatic potential is of prime importance in zeolite science as it governs the site selectivity for the charge compensating cations and the adsorption of guest molecules in the porous host. These fundamental properties are related to the ion-exchange and adsorption/separation properties which are at the base of the principal industrial applications of zeolites (water softening, O_2/N_2 , ortho/meta/para-xylene separation). In this context, its evaluation in Na-X zeolite can serve two goals: evaluation of the interactions inside this peculiar, guest-free zeolite [Aubert *et al.,* 2004], and calculation of potential-

derived atomic charges, suited for a more general modelling of the guest/host interactions by a simple electrostatic model, by molecular dynamic or Monte-Carlo simulations and references therein. We focus here on the second point and consider the evaluation of electrostatic interaction of cations and water molecules in Na-X.

In such a disordered system as Na-X, the conventional calculations of the Coulomb potential [Stewart, 1979], [Becker & Coppens, 1990] are not relevant, and the appropriate method to simulate macroscopic properties is to optimise large number of (Na3, Na4) distributions, possibly in a supercell, and average their properties. Because of computational cost, the electrostatic potential was calculated here for only one such configuration. In that configuration, 16 cations Na3 and 16 Na4 were selected among the 96 of each type. The cation distribution was chosen to avoid energetically unfavourable Na3-Na4 contacts (d > 3.7 Å), and the creation of a dipolar moment in the P1 unit cell.

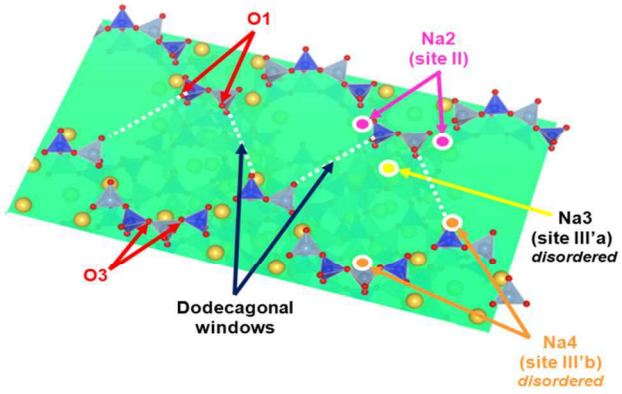

(a)

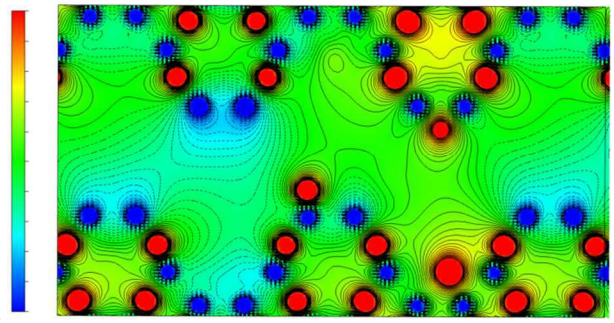

(b)

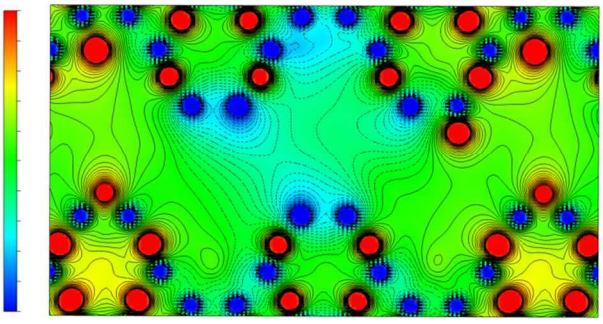

(c)

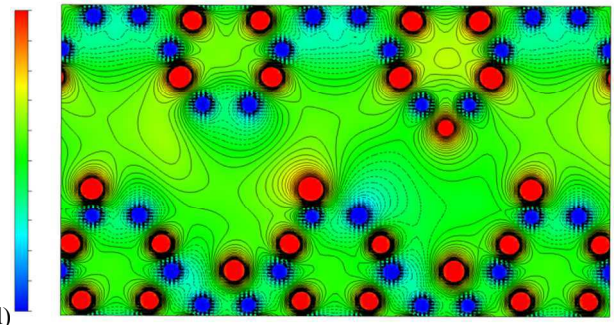

(d)

Fig. 6 Schematic view of the zigzag channels with Na3 and Na4 cations positions and three views of the electrostatic potential in the channels. Minimum and maximum values displayed are -10 (blue) and +10 e/Å (red), and contours lines are 0.5e/Å. The electrostatic potential is calculated with P_{val}-κ charges.

Fig 6a presents a schematic view of the zeolite zigzag channel along [111] direction with the position of disordered cation sites Na3 and Na4. Fig. 6b-d present the electrostatic potential calculated with GULP program [Gale & Rohl, 2003] using P_{val}-κ type point charges (Table 4, CRM[2] lined) for different local Na3, Na4 cation distributions. These views illustrate the potential calculated in different areas of the channels when the local configuration is respectively depleted (Fig 6b), intermediate (Fig. 6c) or rich (Fig 6d) in cations.

When neighbouring sites of dodecagonal windows are vacant, the oxygen atoms that point out the walls generate pockets of negative electrostatic potential (in blue on Fig 6). These pockets precisely sit at site IIIa and IIIb, in those sites more distant from the positions occupied by Na3 or Na4 in that configuration, which became the most attractive sites and are prone to be filled.

The electrostatic energy of individual sites in the configurations shown on Fig. 6 can be evaluated from the electrostatic potential. The most favourable sites have similar average electrostatic potential value (-3 to -4 e/Å) and electrostatic energy (4000 to 5000 kJ/mol for Na^+). This value is about 10 times larger than that calculated by Goursot *et al.* in Na-X using atomic charges of -1.2 for O, +1.4 for Al, +2.4 for Si, and +1.0 for Na [Goursot *et al.*, 1997]. It is, of course, larger than the "global" site IIIa/IIIb energy which has to be averaged over all empty sites, and averaged also on a large set of cation distributions.

However, the similar attractiveness of these sites explains qualitatively the almost identical occupancy factors of Na3 and Na4 in the crystal structure. As the potential is very flat in the channels, with a barrier of only few 10^{-1}e/Å (E~ few 100kJ/mol) at the dodecagonal window, the mobility of the cations is not impeded and hoping between sites IIIa or IIIb is possible. This is in line with the dielectric relaxation experiment of Simon & Flesch [Simon & Flesch, 1999] who evaluated the activation energy for the hopping to ~20kJ/mol for movement inside a supercage, and to ~80kJ/mol if the dodecagonal window is to be crossed.

Concerning the adsorption of guest molecules, this experimental electrostatic potential is only meaningful for small

molecules that do not modify the cation distribution and/or cause the relaxation of the framework. Hence, extrapolation to the adsorption of water molecules in the vicinity of Na3 or Na4 cations is disputable, but has sense for Na2 whose environment is almost unaffected by hydration, as the electric field at adsorption sites is the gradient of the electrostatic potential. For polar molecule like H_2O, one can predict the location of these sites from the expected Na…O approaching distance (typically 2.5Å) and from the dipolar electrostatic energy of H_2O which has to be minimised, hence leading the dipolar moment of the water molecule to align with the electric field.

Table 5 compares the electric field value around cation site II and site III, estimated from the electrostatic potential maps, with values from the literature.

Table 5 Electric field at adsorption sites around accessible cations in Na-X zeolite.

	Handbook of Zeolite Science and Technology (2003)			
	Electrostatic field (V/Å) at distance d from site II		Electrostatic field (V/Å) at distance d from site III	
d(Å)	1.75	2.5	1.75	2.5
E (Na^+)	0.43	0.096	1.11	0.43
	High resolution XRD			
	Electrostatic field (V/Å) at distance d from site II		Electrostatic field (V/Å) at distance d from site III'	
d(Å)	1.8	2.5	1.8	2.5
E(Na^+)	34	8	~42	28

The values calculated from the P_{val}-κ charges are some 80 times larger than those commonly accepted; and 2.6 times larger than that (~3 V/Å) derived with the same method in Natrolite [Ghermani *et al.,* 1996]. As predicted by Shirono *et al.* [Shirono, Endo, & Daiguji, 2005], the electric field is lower in the vicinity of Site II cations than Site III' ones, which will be the first solvated. According to these authors, the adsorption enthalpy of water molecules in Na-X varies from 120 to 70 kJ/mol when the hydration rises from 0 to 220 kJ/mol. With our point-charges model, the electrostatic energy of a water molecule with a ~2D dipole moment trapped in the electric field (E~28 V/Å) of a Na3 cation would be approximately 1300 kJ/mol. This value is 10 times larger than what expected, but the calculation of Shirono *et al*. is done at an average site III position intermediate between site III'a and III'b and with longer Na-O distances, and includes a Lennard-Jones type correction. For Na2, which is more tightly coordination to framework oxygen atoms, a pure electrostatic calculation leads to an energy of 370 kJ/mol, less than 6 times the lower predicted energy. Abrioux *et al.* [Abrioux *et al.,* 2009] draw exactly the same conclusions (solvation of site III' cations prior to that in sites II, hydration-induced displacement of cations in site III' but not in site II) from combined Monte-Carlo and Molecular Dynamics Simulations.

Conclusions

This study presents for the first time the experimental charge density of the Na-X zeolite. Sensible atomic charges are obtained in this rather complex and flexible zeolite, which compare well with the literature and with our test study on α-quartz [Porcher, 2012]. A simple point-charges model of the electrostatic potential, calculated with the P_{val}-κ charges directly refined against Bragg intensities provides qualitatively correct information about cation sites affinities and adsorption sites for water molecules. These charges are extremely close to those derived by Mortier *et al*. [Mortier *et al*., 1986] using the Electronegativity Equalization Method which have proven to be well adapted for the modelling of cation exchange and adsorption in industrial zeolites [Di Lella *et al*., 2006]; [Jeffroy *et al*., 2011]. This trend is confirmed with the experimental study of electrostatic properties of silicalite (zeolite framework-type MFI) [Porcher, 2012].

Acknowledgements

The authors acknowledge the support of the European Synchrotron Radiation facility and the Service Commun de Diffraction X of Université de Lorraine (Nancy, FRANCE) for access to X-Ray facilities.

Notes and references

[a] Cristallographie, Résonance Magnétique et Modélisations, CRM^2, UMR7036 CNRS-UHP, Faculté des Sciences, Université de Lorraine, BP 70239, 54506 Vandœuvre-lès-Nancy Cedex, France E-mail florence.porcher@cea.fr Fax: +33 169088261; Tel: +33 169089373.

[b] Laboratoire Léon Brillouin UMR12 CEA-CNRS, CEA/Saclay, 91191 Gif-sur-Yvette Cedex, France.

Electronic Supplementary Information (ESI) available: [details of any supplementary information available should be included here]. See DOI: 10.1039/b000000x/

1 H. Ramanan, S. M. Auerbach & M. Tsapatsis, *J. Phys. Chem.* 2004, **B(108)**, 17171;
2 A. Wender, A. Barreau, C. Lefebvre, A. Di Lella, A. Boutin, P. Ungerer & A. H. Fuchs. *Adsorption science & technology*, 2006, **24**, n°8, 713;
3 W. Löwenstein, *Am. Mineralogist*, 1954, **39**, 92;
4 G. H. Kühl, *Zeolites*, 1987, **7**, 451;
5 J. F. Charnell, *J. Cryst. Growth*, 1971 **8**, 291;
6 F. Porcher, *Thesis dissertation, Université H. Poincaré Nancy I*, 1998;
7 R. H. Blessing, *Acta Cryst*., 1995, **A51**, 33;
8 V. Petricek, M. Dusek & L. Palatinus, *Jana2006. The crystallographic computing system*, Institute of Physics, Praha, Czech Republic, 2006;
9 P. Coppens, *X-Ray charge density and chemical bonding*, OUP USA/International Union of Crystallography, 1997;
10 M. Sakata & M. Sato, *Acta Cryst*., 1990, **A46**, 263;
11 R. Y. de Vries, W. J. Briels, D. Feil, G. te Velde & E. J. Baerends, *Can. J. Chem*., 1996, **74**: 1054;
12 R. F. Stewart, *J. Chem. Phys*., 1969, **51**, 4569;
13 N. K. Hansen & P. Coppens, *Acta Cryst*., 1978,**A34**, 909;
14 A. T. Brünger, *Nature*, 1992, **355**, 472;

15 B. Zarychta, J. Zaleski, J. Kyzioł, Z. Daszkiewicz & C. Jelsch, *Acta Cryst*., 2011, **B67**, 250;
16 N. E. Ghermani, C. Lecomte & Y. Dusausoy, *Phys. Rev*., 1996, **B9**, 5231;
17 S. Kuntzinger, N. E. Ghermani, Y. Dusausoy & C. Lecomte, *Acta Cryst*., 1998, **B54**, 819;
18 N. Pérès, A. Boukhris, M. Souhassou, G. Gavoille & C. Lecomte, *Acta Cryst*., 1999, **A55**, 1038;
19 F. Porcher, M. Souhassou, Y. Dusausoy & C. Lecomte, *Eur. J. Mineral*., 1999, **11**, 333;
20 A. Kirfel, & G. V. Gibbs, *Phys Chem Minerals*, 2000, **27**, 270;
21 R. W. F. Bader, *Atoms in molecules. A quantum theory*, Plenum Press, Oxford, England University Press, 1990;
22 M. Souhassou & R. H. Blessing, *J. Appl. Cryst*. 1999, **32**, 210;
23 G. V. Gibbs,1, A. F. Wallace, D. F. Cox, R. T. Downs, N. L. Ross & K. M. Rosso, *Am. Mineralogist*, 2009, **94**, 1085;
24 W. J. Mortier, S. K. Ghosh & S. Shankar, *J. Am. Chem. Soc*., 1986, **108**, 4315;
25 L. Uytterhoeven, D. Dompas & W. J. Mortier, *J. Chem. Soc. Faraday Trans*., 1992, **88(18),** 2753;
26 A. Di Lella, N. Desbiens, A. Boutin, I. Demachy, P. Ungerer, J-P. Bellat & A. H. Fuchs, *Phys. Chem. Chem. Phys*. 2006, **8**, 5396;
27 R. Guillot, *Thesis dissertation*, Université H. Poincaré Nancy I, 2002;
28 G. V. Gibbs, K. M. Rosso, D. M. Teter, M. B. Boisen Jr., M. S. T. Bukowinski, *J. Mol. Struct*, 1999, **vol. 485, n°1-3,** 13;
29 E. Aubert, F. Porcher, M. Souhassou, C. Lecomte, *J. Phys. Chem. Solids*, 2004, **65** 1943;
30 R. F. Stewart, *Chem. Phys. Lett*., 1979, **vol 67**, 2, 335;
31 P. Becker & P. Coppens, *Acta Cryst*. 1990, **A46**, 254;
32 J. D. Gale & A. L. Rohl, *Mol. Simul*., 2003, **29**, 291;
33 A. Goursot., V. Vasilyev, & A. Arbuznikov, *J. Phys. Chem*., 1997, **B(101)**, 6420;
34 U. Simon, & U. Flesch, *J. Porous Mater.*, 1999, **6**, 33;
35 K. Shirono, A. Endo, & H. Daiguji, *J. Phys. Chem*., 2005, **B(109),** 3446;
36 C. Abrioux, B. Coasne, G. Maurin, F. Henn, M. Jeffroy, A. Boutin, *J. Phys. Chem*. 2009, **C(113)**, 10696;
37 M. Jeffroy, E. Borissenko, A. Boutin, A. Di Lella, F. Porcher, M. Souhassou, C. Lecomte, A. H. Fuchs, *Microporous and Mesoporous Materials*, 2011, **138**, 45;
38 F. Porcher, *Habilitation à diriger des Recherches*, Université de Lorraine, 2012;